

# Influence of nonideal mixing properties on viscous fingering in micropillar array columns

F. Haudin,<sup>1</sup> M. Callewaert,<sup>2</sup> W. De Malsche,<sup>2</sup> and A. De Wit<sup>1</sup>

<sup>1</sup>*Université libre de Bruxelles (ULB), Nonlinear Physical Chemistry Unit, CP 231,*

*Faculté des Sciences, 1050 Brussels, Belgium*

<sup>2</sup>*Department of Chemical Engineering, Vrije Universiteit Brussel (VUB), Pleinlaan 2, 1050 Brussels, Belgium*

(Received 10 May 2016; published 1 November 2016)

Miscible viscous fingering is studied experimentally in the presence of a nonmonotonic viscosity profile due to nonideal mixing properties in a porous medium consisting in a micropillar array column used for chromatographic applications. In this setup, a mobile phase composed of an aqueous solution of methanol displaces a miscible finite-size sample containing mainly water. Due to a local buildup by nonideal mixing of maxima in the viscosity profile, fingering is observed at both the frontal and rear miscible interfaces of the sample phase, however with different spatial extents. The influence on the fingering dynamics of the pressure in the column and of the viscosity of the mobile or sample phases is analyzed.

DOI: [10.1103/PhysRevFluids.1.074001](https://doi.org/10.1103/PhysRevFluids.1.074001)

## I. INTRODUCTION

Viscous fingering (VF) is a hydrodynamic instability that occurs in porous media when a less viscous fluid is injected in a more viscous one and affects both immiscible and miscible displacements [1,2]. It is relevant in numerous applications such as oil recovery, CO<sub>2</sub> injection in soils, or chromatographic separations, to name a few. Numerous experimental and theoretical studies have been devoted to analyze the properties of the related fingering dynamics.

In the miscible displacement case, the viscosity  $\mu$  of the fluids at hand is typically a function of the concentration  $c$  of a given solute like in the case of water-glycerol mixtures, for instance [3,4]. When water is injected into the miscible more viscous glycerol, the viscosity profile (i.e., the viscosity as a function of space) increases monotonically in the direction of injection and a fingering instability develops at the miscible water-glycerol interface. Such miscible VF with monotonic profiles has been largely studied theoretically [1,5,6] considering typically a solution in concentration  $c_1$  of the viscosity-controlling solute displacing a more viscous miscible solution in which the concentration  $c = c_2$ . In that case, an important parameter of the related modeling is the mobility ratio  $R = \mu_2/\mu_1$  quantifying the ratio of the viscosities  $\mu_2 = \mu(c = c_2)$  and  $\mu_1 = \mu(c = c_1)$  of the displaced and injected solutions, respectively. Viscous fingering sets in when  $R > 1$  and the larger its value, the more intense the fingering. The reverse case of a viscous fluid invading a less viscous one ( $R < 1$ ) is stable in the case of a monotonically decreasing viscosity profile.

Recently, it has been shown both experimentally [7] and theoretically [8,9] that the buildup of nonmonotonic viscosity profiles due to a chemical reaction could induce a destabilization of a more viscous phase displacing a less viscous one. Similarly, precipitation reactions can induce fingering patterns due to a nonmonotonic change in permeability and hence mobility [10–12]. In colloidal suspensions, fingering due to a local increase of the effective viscosity has been evidenced as well [13]. Such nonmonotonic viscosity profiles can also typically be obtained in a large class of nonideal solutions. In such nonideal systems, the molecular interactions between different molecules of the mixture are not the same as the interactions between molecules of the same type. As a result,  $\mu(c)$  can be a nonmonotonic function of  $c$ , i.e., such that the viscosity features an extremum value  $\mu_m$  for an intermediate mass fraction  $c_m$  of one of the fluids. We will hence refer here to nonideal mixing as mixing between two fluids exhibiting nonideal properties with an extremum in viscosity at an intermediate concentration. Examples of such nonideal mixtures and their physical properties are well documented in the literature [14–17]. For instance, water-alcohol mixtures have a viscosity

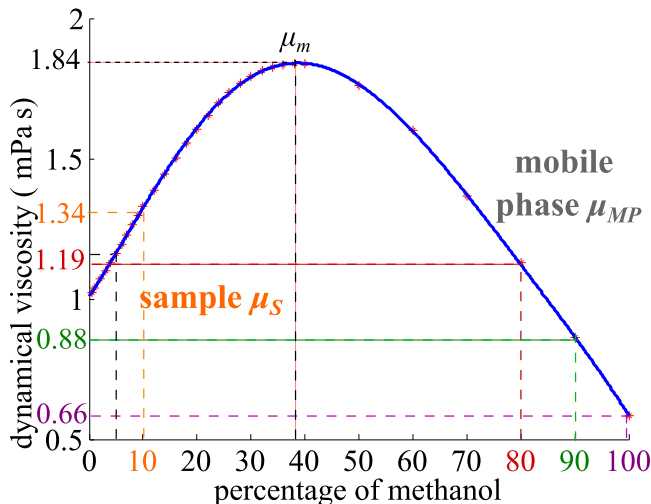


FIG. 1. Dynamic viscosity of water-methanol solutions as a function of the percentage in mass of methanol. The solid line is a polynomial fit of the data from Ref. [14] shown by red asterisks. The viscosity values reported on the vertical axis correspond to the measured viscosity of the sample when containing 10% methanol ( $\mu_s = 1.34$  mPa s) and the viscosity of the dyed mobile phase with 80%, 90%, or 100% methanol ( $\mu_{MP} = 1.19$ , 0.88, or 0.66 mPa s, respectively).

that varies nonmonotonically with the concentration  $c$  of the alcohol [18]. Figure 1 shows the viscosity-concentration relationship of a nonideal water-methanol mixture that features a maximum  $\mu_m$  in viscosity at an intermediate composition  $c_m$  in methanol. Such nonideal mixing properties are particularly important in chromatographic applications for which water-methanol solutions of different composition are sometimes used as the mobile phase and sample solvent [19,20]. Such nonideal effects have also been evidenced in microfluidic devices, for instance, where nonideal mixing of water and ethanol in T-junction mixers have been shown to affect mixing efficiency [17]. Nonmonotonicity in mobility is also particularly relevant for cosolvent floods in aquifer media involving NAPLs (nonaqueous phase liquids) [18,21,22] and for surfactant alternating gas (SAG) foam enhanced oil recovery techniques [23,24]. In these applications, local extrema of viscosity can develop due to nonideal mixing which can potentially induce hydrodynamic fingering instabilities. It is of interest to understand the impact on the fingering dynamics of the nonmonotonic viscosity profile developing upon mixing of the nonideal mixture components.

Numerous theoretical and numerical works have analyzed the properties of viscous fingering with nonmonotonic viscosity profiles due to nonideal mixing properties. It was first recognized a long time ago that any segment of decreasing mobility is linearly unstable [25,26]. Successive linear stability analyses [27–30] have suggested that, in the case of a nonmonotonic profile between the two end-point values  $\mu_1$  and  $\mu_2$  of the invading and displaced solutions, respectively, the parameter  $R$  is not an adequate quantity. Indeed, the stability criteria at initial time are influenced by the end-point derivatives of viscosity with respect to concentration or molar fraction  $c$  and the parameter proposed to estimate the stability of the initial situation is  $\Lambda$ , which is defined as

$$\Lambda = \left[ \frac{(d\mu/dc)|_{c=c_1} + (d\mu/dc)|_{c=c_2}}{\mu_1 + \mu_2} \right], \quad (1)$$

where the subscripts 1 and 2 refer to the invading and displaced fluids, respectively, with  $c_1$  and  $c_2$  the concentrations of the solute affecting the viscosity of the carrier fluid in the related phase. By convention  $\Lambda > 0$  ( $\Lambda < 0$ ) corresponds to an unstable (a stable) case.

Nonlinear simulations, however, have shown that, even if a negative  $\Lambda$  at time  $t = 0$  means an initially stable system for the step concentration profile, dispersion and mixing of the two fluids can induce instability later on when the base state diffuses out [29,30]. This also suggests that nonmonotonic profiles can be stable at  $t = 0$ , even when the end-point viscosities represent an overall unfavorable profile [31]. The parameter  $\Lambda$  is thus not helpful to characterize the dynamics at later times once diffusion comes into play and a nonmonotonic viscosity profile builds up in space.

Nonlinear simulations in a rectilinear geometry have in addition shown that reverse fingering, where the fingers spread preferentially in the backward rather than in the forward direction, typically characterizes the dynamics in the presence of nonmonotonic viscosity profiles [32,33]. This phenomenon due to the stable barrier inhibiting the forward growth of fingers is also typically seen in reactive fingering with a maximum in the viscosity profile [7,9]. Pankiewicz and Meiburg have extended the analysis of nonmonotonicity to the quarter five spot geometry showing that it can lead to a larger recovery rate [31].

Interestingly, Schaefroth *et al.* [34] have further shown with three-dimensional (3D) nonlinear Stokes simulations that nonmonotonicity effects have a much smaller influence in Hele-Shaw Poiseuille flows than on corresponding real porous media Darcy flows. This is related to the fact that, for Darcy flows, the base state is characterized by a constant velocity and a diffusively decaying concentration (and hence viscosity) profile, while for Hele-Shaw displacements, the base states rather feature sharp fronts. Their shape depends only weakly on the details of the viscosity-concentration relationship and hence growth rates for nonmonotonic fingering are similar to those of the monotonic cases. This result might explain why direct visualization of nonmonotonic VF due to nonideal mixing in the absence of reaction has been lacking as it appears to be of small influence in Hele-Shaw cells and difficult to study in real porous media [18].

In this context, De Malsche *et al.* [35] have recently shown that micropillar array columns developed for liquid chromatography applications [35–37] are useful porous systems to study and visualize viscous fingering properties. The onset and extent of viscous fingering as well as its impact on the separation efficiency were studied by displacing small sample bands of pure methanol by mixtures of 0–50 % water in methanol. In that situation, the viscosity profile develops monotonically in space and only one unstable interface develops at either the frontal or the rear region of the plug. The advantage of such micropillar systems is an easy visualization of the fingering dynamics, without the need for mobile phase adjustments to enable optical density matching as previously done in 3D porous media [38]. The channels also offer the possibility to follow the dynamics of a sample over very long distances.

Using such micropillar array columns, we investigate here experimentally the influence of nonideal mixing properties on viscous fingering of water-methanol displacements for which nonmonotonic viscosity profiles develop over the course of time. We demonstrate experimentally that, in the presence of maxima in the viscosity profile, a VF instability can develop simultaneously on both the frontal and rear interfaces of the injected sample. To do so, we analyze the properties of fingering in the presence of related nonmonotonic viscosity profiles both when the less viscous fluid displaces the more viscous one and in the reverse case. We show that fingering develops in both cases with, however, different spatial extents. Fingers extend preferentially in the backward direction as expected for a fingering involving a maximum in the viscosity profile. We further analyze the influence on the dynamics of the pressure in the column and of the viscosity of either the sample or the mobile phase.

The article is organized as follows. Section II describes the experimental setup and visualization techniques. Section III explains the nonideal mixing properties of the sample and mobile phases used in the displacement and discusses the evolution of the viscosity profile in time. Section III describes the viscous fingering properties observed experimentally. A parametric study of the dynamics is conducted in Sec. IV to analyze the influence of the pressure and of the end-point viscosities on the spreading of the fingered zone. Section IV summarizes.

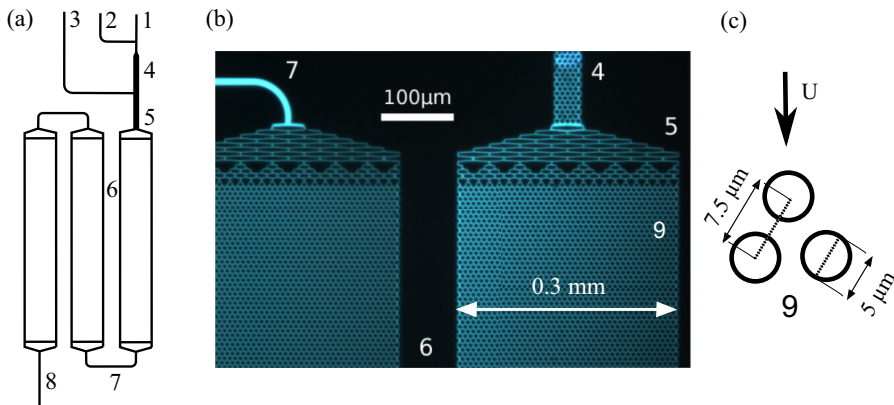


FIG. 2. (a) Schematic representation of a micropillar setup for a 0.3-mm-wide column, (b) microscope image of the selected area, and (c) dimensions of a typical pillar array filling the lanes, with the large arrow indicating the flow direction. The different numbers correspond, respectively, to 1, the inlet for the mobile phase; 2, the inlet for the sample phase; 3, the outlet for the sample phase; 4, the injection box; 5, the inlet distributor; 6, the channel track; 7, the connecting turn; 8, the outlet of the mobile phase; and 9, the micropillars.

## II. MICROPILLAR SYSTEMS

The experiments are performed in silicon (nonporous, not coated)  $5 \mu\text{m}$  in diameter micropillar array columns as used by Callewaert *et al.* [36] for chromatographic purposes. A schematic diagram of a column is shown in Fig. 2(a). The advantage of such chromatographic columns is that dispersion is very low and the displacement can be followed over very long distances. Moreover, such chips are covered with pyrex glass, which makes it possible to follow the dynamics inside the chip by direct imaging using fluorescence microscopy.

The system features two nitrogen pressurized vessels containing, respectively, the mobile phase and the sample, each controlled by a pressure reducer. The connection between the vessels and the column is obtained using  $150 \mu\text{m}$  in diameter capillaries, while liquid injection and displacement are ensured by external valves. Figure 2(b) shows a microscopy image of such a micropillar column. We use here a 1-mm-wide chip on which more than one finger can be observed in the width of the system. The column is filled with a mixture of methanol and water referred to as the mobile phase (MP) with viscosity  $\mu_{\text{MP}}$ . A long plug of fluid is then injected in the mobile phase. This plug, referred to as the sample  $S$  with viscosity  $\mu_S$ , contains a different amount of methanol than the mobile phase (Table I and Fig. 3).

The solutions are prepared from a given weighted mass of pure methanol. Milli-Q water is next added to it to obtain the targeted mass fraction of methanol. Fluorescent coumarin dye is added to the mobile phase for visualization purposes. We have checked that the dye does not change the viscosity much (see Table II). The micropillar device is placed on a translation stage driven by a computer that allows to us track the sample displacement. Once a reference origin is defined, controlled

TABLE I. Viscosities  $\mu_S$  of samples measured with a viscometer in the absence of any dye and related mobility ratios for different sample compositions and a 85% methanol mobile phase with viscosity  $\mu_{\text{MP}} = 1.10 \text{ mPa s}$  and  $\mu_m = 1.84 \text{ mPa s}$ .

Methanol content in $S$	$\mu_S$ (mPa s)	$R_u^b = \mu_m / \mu_{\text{MP}} = 1/R_s^f$	$R_u^f = \mu_m / \mu_S = 1/R_s^b$
0%	1.01	1.67	1.82
10%	1.34	1.67	1.37

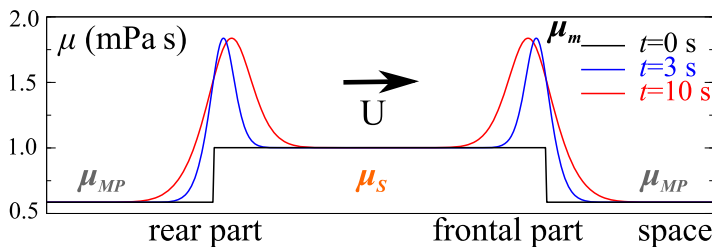


FIG. 3. Theoretical viscosity profiles at different times for a displacement of a sample of pure water sandwiched in a pure methanol mobile phase.

displacements of the chip to successive positions  $x_{\text{pos}}$  are performed: The dynamics of both the frontal and rear parts of the plug are thus recorded in the given field of view with a fixed camera. Visualization is made due to an inverted microscope. A double pass filter allows blue light (501 nm) to excite the fluorescent dye and blocks any other light except the green fluorescent signal light (555 nm). A Hg-vapor lamp is used as a light source and an air-cooled high-speed CCD camera (Hamamatsu Photonics K.K., Japan) is used to produce the images. The fluorescence intensity distributions are subsequently recorded using the accompanying HCIMAGELIVE image analysis software and analyzed using MATLAB.

### III. NONIDEAL FLUID MIXING PROPERTIES

The experiments consist in displacing in the micropillar column at a given speed  $U$  a plug of the sample  $S$  sandwiched in the mobile phase MP. Figure 3 shows the theoretical viscosity profiles that develop over time in the case of a sample of pure water with viscosity  $\mu_S = 1$  mPa s displaced in a mobile phase of pure methanol ( $\mu_{\text{MP}} = 0.66$  mPa s). These profiles are obtained by computing the profile  $\mu(x, t)$  using the data of Fig. 1 and the error function  $c(x, t)$ , the solution of the diffusive equation for the mass fraction  $c$  of methanol for the initial and boundary conditions shown in Fig. 3.

We note that, in all experiments, the length of the sample is much larger than the extent of the fingering zones, so the dynamics of the frontal and rear parts of the sample are independent. We are thus able, during one experiment with a plug, to analyze the dynamics of both frontal and rear parts as the dynamics of two independent semi-infinite zones.

In our experiments, the frontal part of the plug typically corresponds to a water-rich sample solution displacing a less viscous methanol richer mobile phase, a situation with  $R < 1$  (see Tables I and II), which is initially stable. However, as suggested by previous numerical works [33], once the two fluids start mixing, a zone with a maximum viscosity  $\mu_m$  develops and reverse fingering, triggered by this nonideal mixing effect, can take place in the zone where  $\mu_S < \mu_m$ . In the following we will refer to this fingering induced by nonideal effects for an initially stable case where  $R < 1$

TABLE II. Measured viscosities  $\mu_{\text{MP}}$  of the mobile phases with or without a dye and related mobility ratios for different mobile phase compositions. The sample is a solution of 10% methanol with viscosity  $\mu_S = 1.34$  mPa s and  $\mu_m = 1.84$  mPa s.

Methanol content in MP	$\mu_{\text{MP}}$ dyed (mPa s)	$\mu_{\text{MP}}$ undyed (mPa s)	$R_u^b = \mu_m / \mu_{\text{MP}} = 1 / R_s^f$	$R_u^f = \mu_m / \mu_S = 1 / R_s^b$
100%	0.63	0.66	2.92	1.37
90%	0.88		2.09	1.37
85%	1.10		1.67	1.37
80%	1.19	1.26	1.55	1.37

as nonideal  $\text{VF}_s$ . At the rear interface of the plug, the less viscous mobile phase displaces the more viscous sample and hence  $R > 1$ . This initially unstable case will be referred to as nonideal  $\text{VF}_u$  in the rest of the paper. Our objective here is to investigate the difference between these two nonideal VF cases as a function of the parameters of the problem, which are the pressure applied in the column and the composition of the MP and sample, respectively.

To compare properties of different displacements, we introduce the mobility ratios  $R_u^b$  and  $R_u^f$  characterizing the unstable back (superscript  $b$ ) and stable forward (superscript  $f$ ) part of the nonmonotonic viscosity profile at the initially unstable (subscript  $u$ ) rear interface where the less viscous MP displaces the more viscous sample ( $R > 1, \text{VF}_u$ ). They are defined as

$$R_u^b = \frac{\mu_m}{\mu_{\text{MP}}}, \quad R_u^f = \frac{\mu_S}{\mu_m}. \quad (2)$$

Similar quantities  $R_s^b$  and  $R_s^f$  can be defined to quantify the viscosity jumps in the unstable back ( $b$ ) and stable forward ( $f$ ) part of the initially stable ( $s$ ) frontal interface where the more viscous sample displaces the less viscous MP ( $R < 1, \text{VF}_s$ ) i.e.,

$$R_s^b = \frac{\mu_m}{\mu_S}, \quad R_s^f = \frac{\mu_{\text{MP}}}{\mu_m}. \quad (3)$$

By symmetry,  $R_u^b = 1/R_s^f$  and  $R_u^f = 1/R_s^b$ . Tables I and II report the viscosities [14] of the various sample and mobile phase solutions used in the experiments as well as the related different values of viscosity ratios.

#### IV. FINGERING AT BOTH THE FRONTAL AND REAR INTERFACES

Due to the long length of the set-up, it is not possible to follow a sample's deformation throughout the column in the course of time. Instead, the camera is fixed at a given distance  $x_{\text{pos}}$  of the inlet to record the spatial distribution of the fluorescence intensity when the sample passes by in the field of view. Let us start looking at the dynamics in a stable case.

##### A. Stable case and data processing technique

To be able to discriminate deformations of the miscible interfaces due to viscous fingering from those induced by lateral wall effects, we first study a stable displacement when the mobile phase and the sample are the same fluids. The dynamics is followed due to the fluorescent tracer added in the MP. As shown in Table II, the presence of this dye does not change the viscosity of the methanol rich phase significantly. A reference picture  $I_{\text{ref}}$  of the fluorescence intensity in the MP is taken before the sample travels in the field of view of the camera [Fig. 4(a)]. After injection of the sample of the same viscosity, a snapshot of its frontal and rear interfaces are recorded [Figs. 4(b) and 4(c), respectively]. To get rid of the inhomogeneities in the light distribution, we apply the following normalization to the images:

$$I_{\text{frontal}}^n = \frac{I_{\text{ref}} - I_{\text{frontal}}}{I_{\text{ref}} - I_{\text{min}}}, \quad (4)$$

$$I_{\text{rear}}^n = \frac{I_{\text{ref}} - I_{\text{rear}}}{I_{\text{ref}} - I_{\text{min}}}, \quad (5)$$

where  $I_{\text{min}}$  is the minimum of  $I_{\text{frontal}}$ . Figures 4(d) and 4(e) show the normalized fluorescence distributions  $I_{\text{rear}}^n$  and  $I_{\text{frontal}}^n$ , respectively, and Fig. 4(f) shows the related transverse averaged normalized fluorescence intensity, which corresponds to the normalized fluorescence intensity averaged over the width of the column. (Note that throughout the text and figures, normalized intensity will stand for transverse averaged normalized fluorescence intensity.) These profiles show that the normalized intensity level goes slightly over 0 on the left for the rear profile due to the fact that  $I_{\text{ref}}$  is locally larger than  $I_{\text{rear}}$ . On the images of the sample interfaces, we can see that sidewall

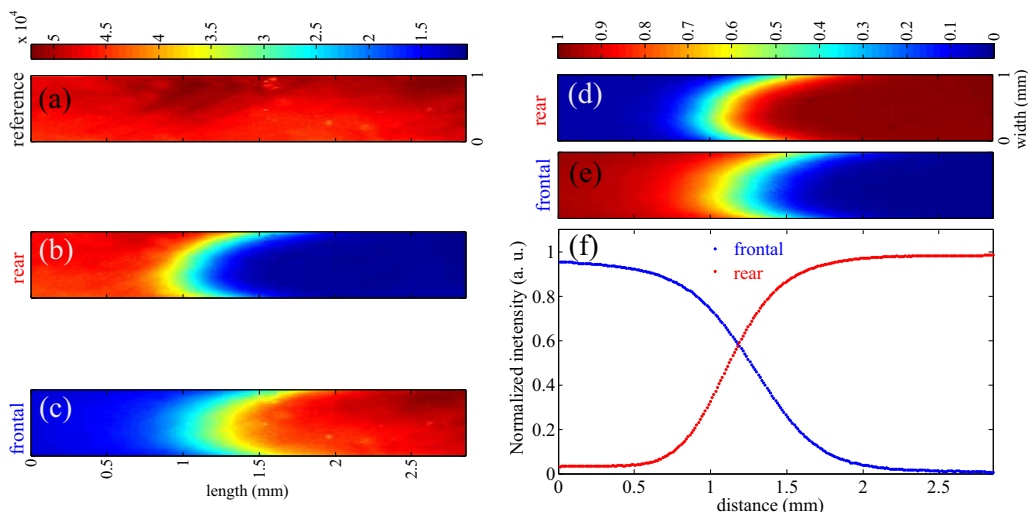


FIG. 4. Spatial distributions of the fluorescence intensity without normalization at a distance  $x_{\text{pos}} = 1.5$  cm from the injection box for (a) a column filled with a MP of 100% methanol, (b) the rear part, and (c) the frontal part of the sample for  $S = 100\%$  methanol and  $P = 20$  bars. Also shown are the normalized spatial distributions of the fluorescence intensity for the (d) rear and (e) frontal parts of the sample plug, respectively. The field of view is  $1 \times 2.85$  mm<sup>2</sup>. (f) Spatial dependence of the transverse averaged normalized fluorescence intensity for both the frontal and the rear parts of the sample plug.

effects exist, leading to similar deformation of the viscously stable sample boundaries at both sides. This is due to the fact that the flow resistance of the channel that is formed between the pillars next to the sidewall is not equal to the one in the central part of the column. Small differences between both zones are often present, resulting in a distorted sample band as observed in previous works [37]. It should be emphasized that the observed profile is not the parabolic flow profile typically obtained in an open tubular channel. Nevertheless, the deformation is the same at both interfaces in the absence of any viscous instability and this stable displacement can thus perfectly serve as a reference state.

### B. Unstable case and repeatability of the experiments

We next analyze the sample deformation when viscosity differences act across the miscible interfaces. To do so, we inject a sample containing 10% methanol ( $\mu_S = 1.34$  mPa s) into a mobile phase 85% rich in methanol ( $\mu_S = 1.10$  mPa s), at a pressure of 20 bars. Figure 5 shows that, in this case, both interfaces are deformed into fingers. The experiment has been performed for five consecutive runs in the same conditions. We can first see that, as previously noticed for such micropillar array columns [35], deformations are very similar for all the runs (Fig. 5). This points to the fact that perturbations at the entrance of the column are largely affecting the deformation. The pressure-driven pumping and injection system equipped with a fast response automated injection valve enable indeed highly reproducible consecutive injections. In agreement with earlier observations [35], the position where the initial disturbance occurs is highly reproducible and enhanced by minor geometrical differences of the injected sample band as well as of the pillar channel itself. Yet concerning the fingering phenomena, one can notice that the fingered pattern is different at the frontal and rear parts of the plug and differs also clearly from the stable displacement (Fig. 4). Moreover, we can see that the fingering deformation is much larger at the rear (overpassing the field of view of the camera) than at the front as confirmed by the normalized fluorescence intensity profiles [Figs. 5(a6) and 5(b6)].

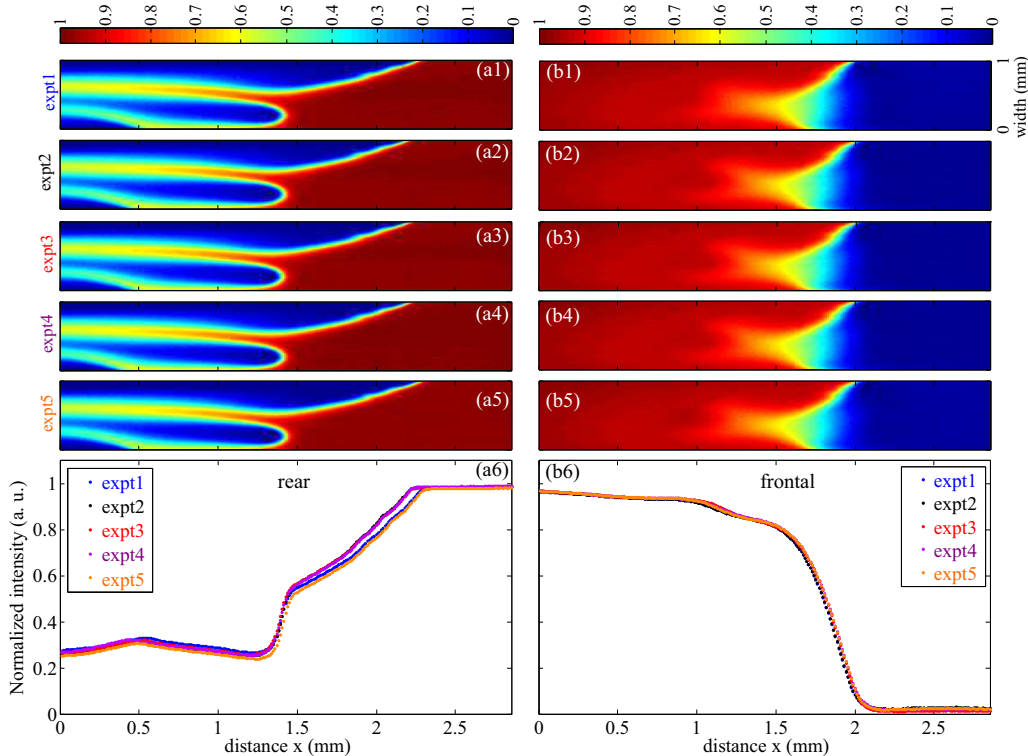


FIG. 5. Spatial distributions of the normalized fluorescence intensity at the (a1)–(a5) rear and (b1)–(b5) frontal parts of the sample plug for five successive experiments in the same experimental conditions. Also shown are the transverse averaged normalized fluorescence intensity profile for the (a6) rear and (b6) frontal parts of the sample plug. The images are taken at a distance  $x_{\text{pos}} = 1.5$  cm from the injection box. Here the MP is 85% and  $S = 10\%$  in methanol and  $P = 20$  bars. The field of view is  $1 \times 2.85$  mm<sup>2</sup>.

### C. Nonideal fingering

To understand the difference in fingering at both interfaces in the case of viscosity contrasts between the sample and the MP (Fig. 5), we recall that, at the rear, the less viscous MP displaces the more viscous sample. Then  $\text{VF}_u$  can develop, which is clearly evidenced by the fingers in the direct view and the bumps and plateau in the transverse averaged profile. Note that, due to the limited field of view with the setup, it is not possible to observe at once the complete mixing zone. Hence, the normalized fluorescence intensity level is not returning to zero at the back. As a signature of the nonideal mixing effect, we note, however, that the fingers extend preferentially towards the back, which can be related to the presence of a maximum in the viscosity profile (see Fig. 3). In the frontal part, fingering is observed as well even if the sample is more viscous than the invaded mobile phase ( $R < 1$ ). The development of the maximum in viscosity during the displacement and mixing of the two phases triggers locally an unfavorable viscosity gradient, leading to nonideal reverse  $\text{VF}_s$ . The mixing length of this frontal fingering zone is smaller than in the rear  $\text{VF}_u$  because the amplitude of the unfavorable viscosity ratio is smaller and needs some time to build up ( $R_u^f = 1.37 < R_u^b = 1.67$ ).

### D. Space-time output and speed of the fingers

In chromatographic applications [35,39] or in opaque columns [18], detectors are usually located at the exit or at given fixed locations along the column to measure the evolution in time of transverse averaged values of the concentration of the species of interest. We perform here a similar

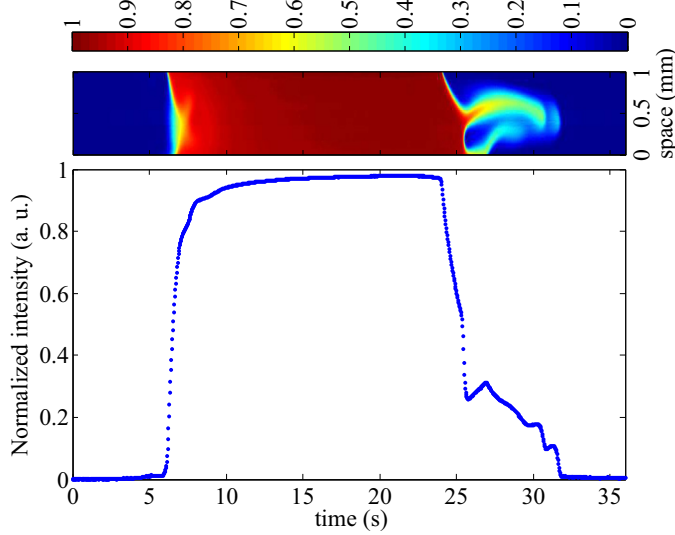


FIG. 6. Shown on top is the space-time plot and on bottom the temporal dependence of the transverse averaged normalized fluorescence intensity at  $x_{\text{pos}} = 1.5$  cm due to the passage of the sample. The MP is 85%,  $S = 10\%$ , and  $P = 20$  bars.

measurement by placing the chip at a given position  $x_{\text{pos}}$  and recording the fluorescence intensity on the width of the channel at this location as a function of time. Figure 6 shows the normalized fluorescence intensity at  $x_{\text{pos}} = 1.5$  cm for the unstable case of Fig. 5, both as a space-time map of the instantaneous measure of fluorescence along the width of the channel (top) and integrated along the width of the channel (bottom). The temporal profile is asymmetric, attesting once more that the

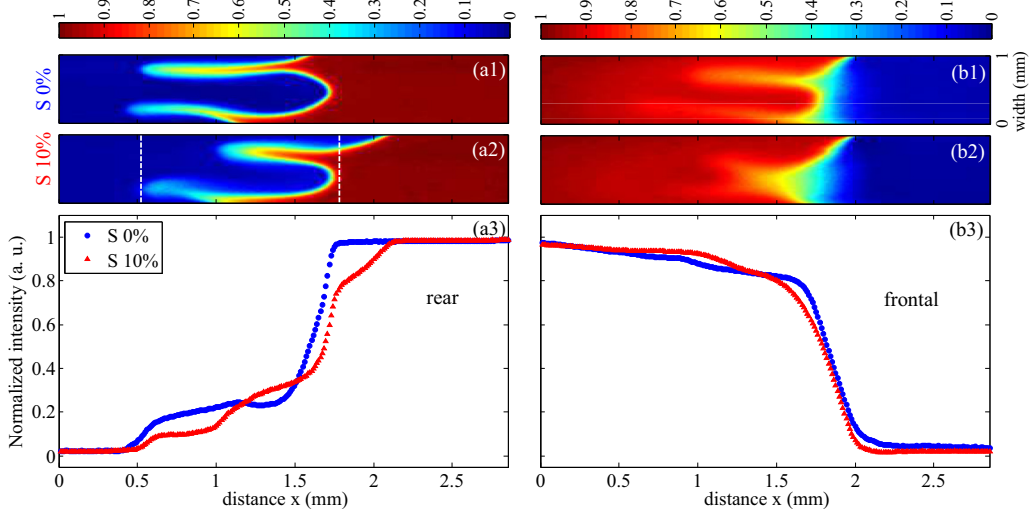


FIG. 7. Spatial distribution of the normalized fluorescence intensity at the (a1) and (a2) rear and (b1) and (b2) frontal parts of the sample plug at a distance  $x_{\text{pos}} = 0.5$  cm (rear) and  $x_{\text{pos}} = 1.5$  cm (front) from the inlet. Transverse averaged normalized fluorescence intensity for the (a3) rear and (b3) frontal parts of the sample plug. The MP is 85%,  $P = 20$  bars, and  $S = 0$  and 10%. The dashed white lines in (a2) evidence the extent of the longest finger in the mixing zone for the less concentrated sample. The field of view is  $1 \times 2.85$  mm<sup>2</sup>.

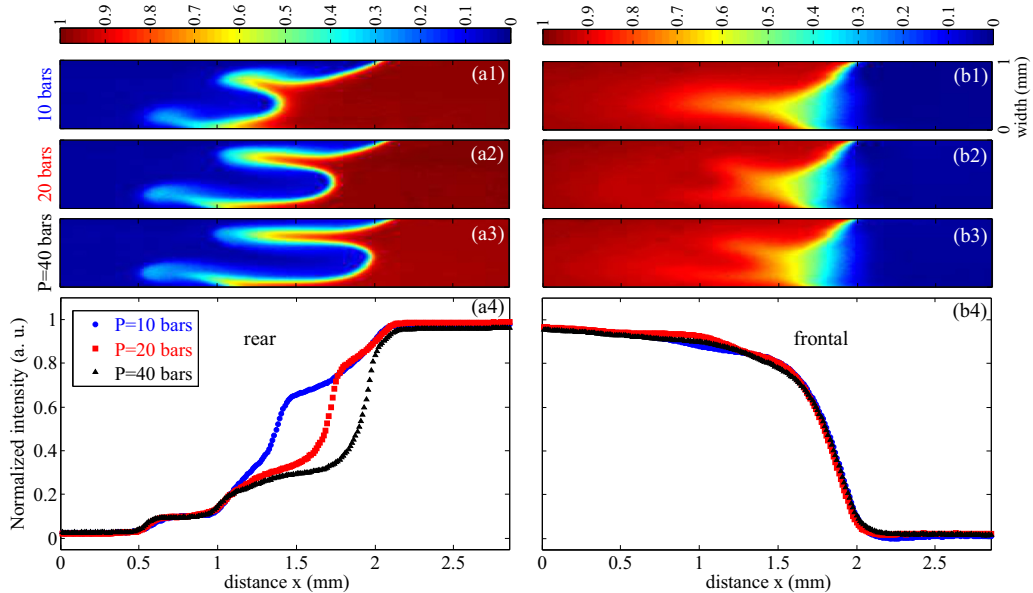


FIG. 8. Spatial distribution of the normalized fluorescence intensity at the (a1)–(a3) rear and (b1)–(b3) frontal parts of the sample plug, at a distance  $x_{\text{pos}} = 0.5$  cm (rear) and  $x_{\text{pos}} = 1.5$  cm (front) from the injection box. Transverse averaged normalized fluorescence intensity for the (a4) rear and (b4) frontal parts of the sample plug. The MP is 85%,  $S = 10\%$ , and  $P = 10, 20$ , or 40 bars. The field of view is  $1 \times 2.85$  mm<sup>2</sup>.

two fingerings are different in the case of viscosity mismatch between the sample and the MP. The fingering is more intense and hence the spreading of the mixing zone is larger at the rear part when  $R > 1$  (later times on Fig. 6) than in the frontal one for which  $R < 1$  (earlier times on Fig. 6).

## V. PARAMETRIC STUDY

### A. Effect of varying the sample concentration

Figure 7 shows fingering of both interfaces for two different sample concentrations. The mobile phase is in all cases composed of 85% methanol ( $\mu_{\text{MP}} = 1.10$  mPa s), while the amount of methanol in the sample equals either 0% or 10%. At the back interface, the unstable jump in the viscosity profile remains the same ( $R_u^b = 1.67$ ) and two fingers are present in all cases. At the frontal part, we see that, for  $S = 0\%$ , there are two fingers of similar amplitude, while one dominant finger is obtained for  $S = 10\%$ . This trend suggests that the situation is more stable when the methanol content of the sample is increased at a fixed composition of the MP. This can be rationalized by looking at Table I, which shows that  $R_u^f$  decreases when the amount of methanol in the sample increases. This means that the unfavorable viscosity ratio in the unstable part of the nonmonotonic viscosity profile at the front becomes weaker at a larger methanol content leading to less intense fingering.

### B. Effect of the pressure in the column

We have also varied the pressure inside the column for a fixed composition of 85% methanol in the MP and 10% methanol in the sample (Fig. 8). The greater the pressure, the larger the extent of the second back finger. We see on the frontal part that, while one finger is obtained at the lowest pressure, a second finger starts to emerge when the pressure is increased. This is in line with the well known

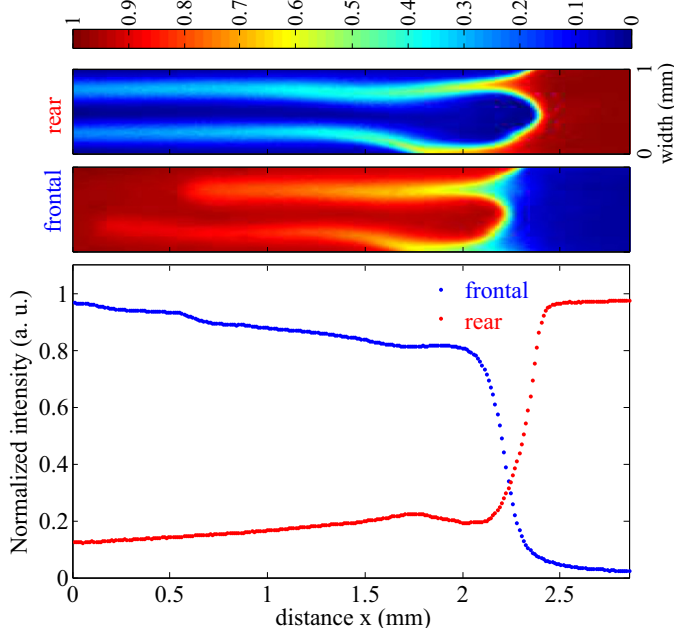


FIG. 9. Spatial distribution of the normalized fluorescence intensity at the (a) rear and (b) frontal parts of the sample plug, at a distance  $x_{\text{pos}} = 1.5$  cm from the injection box. (c) Transverse averaged normalized fluorescence intensity for the rear and frontal parts of the sample plug. The MP is 85%,  $S = 0\%$ , and  $P = 40$  bars. The field of view is  $1 \times 2.85$  mm<sup>2</sup>.

result that, for an unfavorable viscosity ratio ( $R_u^f = 1.67$  here) the system is more unstable and has thus a smaller wavelength when the pressure (and thus the related injection speed) is increased [5].

Figure 9 further shows a very unstable situation when the MP is 85%,  $S = 0\%$ , and  $P = 40$  bars. In that case, the viscosity of the sample is lower than that of the mobile phase. Viscous fingering also develops at both interfaces as the nonmonotonic viscosity profile triggers unfavorable viscosity contrasts in both cases. Note that the spatial extent of both fingerings is comparable, but a bit smaller at the frontal interface.

### C. Effect of varying the MP concentration

To analyze the effect of varying the amplitude of the unstable back part of the viscosity extrema, we also changed the composition of the mobile phase, keeping the amount of methanol in the sample at 10% and the pressure at 20 bars (Fig. 10 and Table II). We see that the longitudinal extent of the fingering increases when the methanol content increases in the MP. This is related to the fact that the viscosity of the MP is then decreasing and that the related unfavorable viscosity ratio  $R_u^b$  increases (see Table II). At the frontal part of the plug, the intensity of fingering slightly decreases even though the unfavorable viscosity ratio  $R_u^f$  remains constant. This can be related to the stabilizing barrier at the front of the extremum ( $R_s^f = 1/R_u^b$ ), which increases when the amount of methanol increases, making it more difficult for the fingers to develop.

## VI. CONCLUSION

We have shown in a column made of micropillar arrays that it is possible to visualize and study experimentally viscous fingering instabilities due to the buildup of a nonmonotonic viscosity profile upon nonideal mixing of solutions of water and methanol. Focusing on the displacement of an

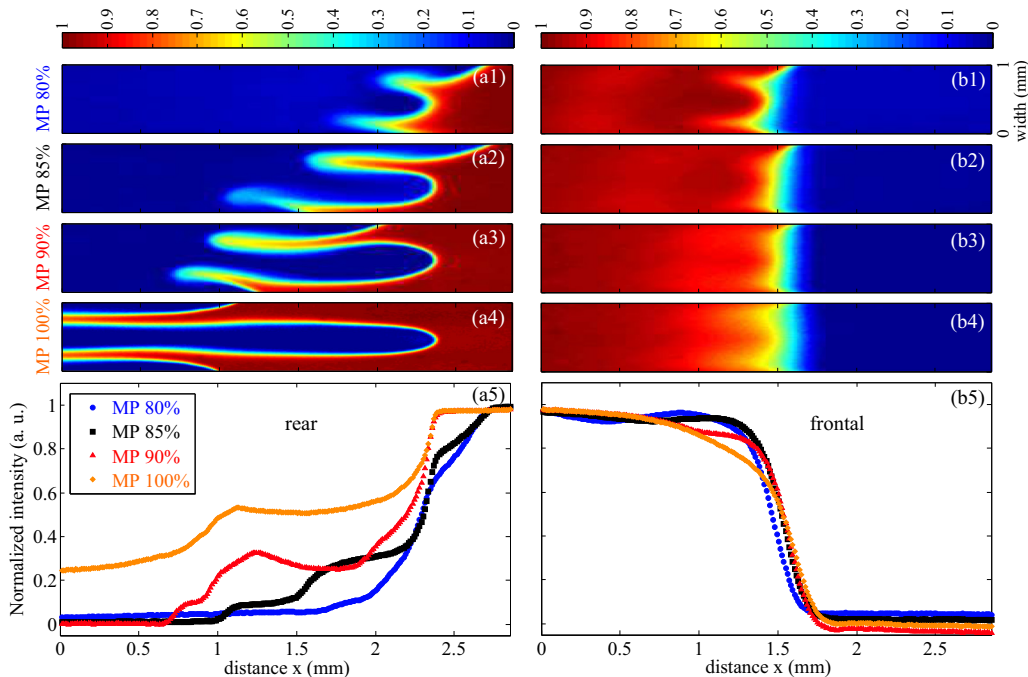


FIG. 10. Spatial distribution of the normalized fluorescence intensity at the (a1)–(a4) rear and (b1)–(b4) frontal parts of the sample plug, at a distance  $x_{\text{pos}} = 0.5$  cm from the injection box. Transverse averaged normalized fluorescence intensity for the (a5) rear and (b5) frontal parts of the sample plug. The variable MP and  $S = 10\%$  and  $P = 20$  bars. The field of view is  $1 \times 2.85$  mm<sup>2</sup>.

aqueous sample containing a small percentage of methanol by a more viscous phase rich in methanol, we have shown that fingering develops at both the frontal and rear parts of the displacement. The experimental observation of VF at the frontal part where  $R < 1$  confirms the theoretical prediction that diffusion destabilizes the system in time by mixing the two solutions, which induces the buildup of a maximum in the viscosity profile. In the rear part, where the less viscous mobile phase displaces the more viscous sample ( $R > 1$ ), the fingers develop with a larger mixing zone than in the frontal part, where  $R < 1$ . This can be explained by the larger viscosity jump in the unfavorable zone of the viscosity profile at the back ( $R_u^b > R_u^f$ ). An increase of the pressure favors fingering. Decreasing the viscosity of the mobile phase by increasing its content in methanol has a destabilizing influence on the rear fingering because the unfavorable viscosity jump  $R_u^b$  increases. In the frontal part,  $R_u^f$  remains constant. Nevertheless, the intensity of the stable barrier increases with the methanol content in the mobile phase, which tends to induce a smaller frontal fingering.

Micropillar arrays have here demonstrated their advantages for studying properties of viscous fingering with nonmonotonic viscosity profiles. The fact that mixing occurs right away in the injection process and dispersion in them is low allows us to follow the influence of nonideal mixing of the two fluids. This is the main advantage with regard to an experiment in a Hele-Shaw cell of classical size [4] in which we could not observe convincing nonideal effects with similar mixtures. It is true that a drawback of the micropillar setup is the need to constantly move the setup in front of the fixed camera to follow the sample during its progression and the limited size of the field of view, which hinders the follow-up of the full extension of the fingers. Nevertheless, the fact that the properties of dispersion within the column can be tailored with the geometry of the pillars [37] makes them a very powerful tool for future comparison of experimental results with theoretical predictions. Our study shows that VF with nonmonotonic viscosity profiles can be successfully studied experimentally and

paves the way for future work to be developed in close comparison with numerical simulations incorporating the specific characteristics of the porous medium and of the nonideal mixtures used.

#### ACKNOWLEDGMENTS

We thank F. Brau and M. Martin for fruitful discussions. A.D. and F.H. thank PRODEX for financial support. A.D. acknowledges support from the FORECAST FRS-FNRS project.

- 
- [1] G. M. Homsy, Viscous fingering in porous media, *Annu. Rev. Fluid Mech.* **19**, 271 (1987).
  - [2] P. G. Saffman and G. I. Taylor, The penetration of a fluid into a porous medium or Hele-Shaw cell containing a more viscous liquid, *Proc. R. Soc. London Ser. A* **245**, 312 (1958).
  - [3] P. Bunton, D. Martin, S. Stewart, E. Meiburg, and A. De Wit, Schlieren imaging of viscous fingering in a horizontal Hele-Shaw cell, *Exp. Fluids* **57**, 28 (2016).
  - [4] R. Maes, G. Rousseaux, B. Scheid, M. Mishra, P. Colinet, and A. De Wit, Experimental study of dispersion and miscible viscous fingering of initially circular samples in Hele-Shaw cells, *Phys. Fluids* **22**, 123104 (2010).
  - [5] C. T. Tan and G. M. Homsy, Stability of miscible displacements in porous media: Rectilinear flow, *Phys. Fluids* **29**, 3549 (1986).
  - [6] C. T. Tan and G. M. Homsy, Simulations of nonlinear viscous fingering in miscible displacement, *Phys. Fluids* **31**, 1330 (1988).
  - [7] L. A. Riolfo, Y. Nagatsu, S. Iwata, R. Maes, P. M. J. Trevelyan, and A. De Wit, Experimental evidence of reaction-driven miscible viscous fingering, *Phys. Rev. E* **85**, 015304(R) (2012).
  - [8] S. H. Hejazi, P. M. J. Trevelyan, J. Azaiez, and A. De Wit, Viscous fingering of a miscible reactive  $A + B \rightarrow C$  interface: a linear stability analysis, *J. Fluid Mech.* **652**, 501 (2010).
  - [9] Y. Nagatsu and A. De Wit, Viscous fingering of a miscible reactive  $A + B \rightarrow C$  interface for an infinitely fast chemical reaction: Nonlinear simulations, *Phys. Fluids* **23**, 043102 (2011).
  - [10] F. Haudin, J. H. E. Cartwright, F. Brau, and A. De Wit, Spiral precipitation patterns in confined chemical gardens, *Proc. Natl. Acad. Sci. USA* **111**, 17363 (2014).
  - [11] Y. Nagatsu, Y. Ishii, Y. Tada, and A. De Wit, Hydrodynamic Fingering Instability Induced by a Precipitation Reaction, *Phys. Rev. Lett.* **113**, 024502 (2014).
  - [12] P. Shukla and A. De Wit, Fingering dynamics driven by a precipitation reaction: Nonlinear simulations, *Phys. Rev. E* **93**, 023103 (2016).
  - [13] H. Tang, W. Grivas, D. Homentcovschi, J. Geer, and T. Singler, Stability Considerations Associated with the Meniscoid Particle Band at Advancing Interfaces in Hele-Shaw Suspension Flows, *Phys. Rev. Lett.* **85**, 2112 (2000).
  - [14] *CRC Handbook of Chemistry and Physics*, 92nd ed., edited by W. M. Haynes (CRC, Boca Raton, 2011).
  - [15] J. B. Irving, *Viscosities of Binary Liquid Mixtures: The Effectiveness of Mixture Equations*, Vol. 631 (National Engineering Laboratory, Great Britain, 1977).
  - [16] M. Moha-Ouchane, C. Bone, A. Allal, and M. Benseddik, Viscosity and excess volume at high pressures in associative binaries, *Int. J. Thermophys.* **19**, 161 (1998).
  - [17] G. Orsi, M. Roudgar, E. Brunazzi, C. Galletti, and R. Mauri, Water-ethanol mixing in T-shaped microdevices, *Chem. Eng. Sci.* **95**, 174 (2013).
  - [18] D. G. Grubb and N. Sitar, Horizontal ethanol floods in clean, uniform, and layered sand packs under confined conditions, *Water Resour. Res.* **11**, 3291 (1999).
  - [19] A. J. Alpert, Hydrophilic-interaction chromatography for the separation of peptides, nucleic acids and other polar compounds, *J. Chromatogr. A* **499**, 177 (1990).
  - [20] C. Horváth, W. Melander, and I. Molnár, Solvophobic interactions in liquid chromatography with nonpolar stationary phases, *J. Chromatogr. A* **125**, 129 (1976).

- [21] T. C. Harmon, T.-J. Kim, B. K. Dela Barre, and C. V. Chrysikopoulos, Cosolvent-water displacement in one-dimensional soil column, *J. Environm. Eng.* **125**, 87 (1999).
- [22] B. P. Stafford, N. L. Cápiro, P. J. J. Alvarez, and W. G. Rixey, Pore water characteristics following a release of neat ethanol onto pre-existing NAPLs, *Ground Water Monit. Remediat.* **29**, 93 (2009).
- [23] R. Farajzadeh, Simulation of instabilities and fingering in surfactant alternating gas (SAG) foam enhanced oil recovery, *Proceedings of the SPE Reservoir Simulation Symposium* (Society of Petroleum Engineers, Richardson, 2015), paper SPE-173193-MS.
- [24] W. R. Rossen, Numerical challenges in foam simulation: A review, *Proceedings of the 14th European Conference on Mathematics in Oil Recovery* (Society of Petroleum Engineers, Richardson, 2013), paper SPE 16624432.
- [25] E. D. Chikhliwala, A. B. Huang, and Y. C. Yortsos, Numerical study of the linear stability of immiscible displacement processes in porous media, *Transp. Porous Media* **3**, 257 (1988).
- [26] F. J. Hickernell and Y. C. Yortsos, Linear stability of miscible displacement processes in porous media in the absence of dispersion, *Stud. Appl. Math.* **74**, 93 (1986).
- [27] J.-C. Bacri, N. Rakotomalala, D. Salin, and R. Wouméni, Miscible viscous fingering: Experiments versus continuum approach, *Phys. Fluids A* **4**, 1611 (1992).
- [28] J.-C. Bacri, D. Salin, and Y. C. Yortsos, Analyse linéaire de la stabilité de l'écoulement de fluides miscibles en milieux poreux, *C. R. Acad. Sci. Paris* **314**, 139 (1992).
- [29] D. Loggia, D. Salin, and Y. C. Yortsos, A note on the effect of dispersion on the stability of non-monotonic mobility profiles in porous media, *Phys. Fluids* **10**, 747 (1998).
- [30] O. Manickam and G. M. Homsy, Stability of miscible displacements in porous media with nonmonotonic viscosity profiles, *Phys. Fluids* **5**, 1356 (1993).
- [31] C. Pankiewitz and E. Meiburg, Miscible porous media displacements in the quarter five-spot configuration. Part 3. Non-monotonic viscosity profiles, *J. Fluid Mech.* **388**, 171 (1999).
- [32] A. L. G. A. Coutinho and J. L. D. Alves, Finite element simulation of nonlinear viscous fingering in miscible displacements with anisotropic dispersion and nonmonotonic viscosity profiles, *Comput. Mech.* **23**, 108 (1999).
- [33] O. Manickam and G. M. Homsy, Simulation of viscous fingering in miscible displacements with nonmonotonic viscosity profiles, *Phys. Fluids* **6**, 95 (1994).
- [34] D. Schafroth, N. Goyal, and E. Meiburg, Miscible displacements in Hele-Shaw cells: Nonmonotonic viscosity profiles, *Eur. J. Mech. B* **26**, 444 (2007).
- [35] W. De Malsche, J. Op De Beeck, H. Gardeniers, and G. Desmet, Visualization and quantification of the onset and the extent of viscous fingering in micro-pillar array columns, *J. Chromatogr. A* **1216**, 5511 (2009).
- [36] M. Callewaert, J. Op De Beeck, K. Maeno, C. Sukas, H. Thienpont, H. Ottevaere, H. Gardeniers, G. Desmet, and W. De Malsche, Integration of uniform porous shell layers in very long pillar array columns using electrochemical anodization for liquid chromatography, *Analyst* **139**, 618 (2014).
- [37] J. Op De Beeck, M. Callewaert, H. Ottevaere, H. Gardeniers, G. Desmet, and W. De Malsche, On the advantages of radially elongated structures in microchip-based liquid chromatography, *Anal. Chem.* **85**, 5207 (2013).
- [38] R. A. Shalliker, H. J. Catchpoole, G. R. Dennis, and G. Guiochon, Visualising viscous fingering in chromatography columns: High viscosity solute plug, *J. Chromatogr. A* **1142**, 48 (2007).
- [39] A. De Wit, Y. Bertho, and M. Martin, Viscous fingering of miscible slices, *Phys. Fluids* **17**, 054114 (2005).